FACOLTÀ DI INGEGNERIA
CIVILE E INDUSTRIALE

SAPIENZA
UNIVERSITÀ DI ROMA

Elaborato finale per il conseguimento
della Laurea in Ingegneria aerospaziale

Modeling Lunar Gravitational Perturbations in Low Orbit Integration

Candidato: Roberto Lucchesi
Matricola: 1744941

Relatore: prof. Antonio Genova
SSD: ING/IND-05

Abstract.
In this paper, two methods for modeling the calculation of perturbations due to the asphericity and non-uniformity of the mass distribution related to the Moon are analyzed. The goal is to optimize the computational integration of low orbits.
A parallel approach to the Pines algorithm is experimented with, as well as an approximate solution considering disks of surface mass concentrations. The results of the analysis are compared with the solutions and computational times of the Pines algorithm for calculating perturbative accelerations.

1. Introduction

Thanks to the NASA Artemis missions, which aim for a long-term presence on the lunar surface, the Moon has gained renewed interest in terms of space exploration. However, to establish the orbital infrastructure required by these missions, one must take into account the strong lunar gravitational perturbations. On the lunar surface, significant mass concentrations, known as *mascons*, cause a substantial perturbation in the gravitational field. It is therefore crucial to consider these perturbations both in the orbital design phase and during the mission.
The Gravity Recovery and Interior Laboratory (GRAIL) mission provided high-precision data, allowing for the appreciation of the non-uniformity of the lunar gravitational field. This enabled the estimation of coefficients in the series expansion of spherical harmonics up to orders and degrees as high as 1200[1], making the Moon the most well-known satellite in terms of gravitational characteristics. Such gravitational model has facilitated the use and prediction of increasingly precise orbital trajectories. Still, the high computational cost makes it challenging to develop high-order spherical harmonics for calculating disturbance accelerations onboard satellites. Therefore, there is significant interest in research and development of algorithms capable of achieving optimal results for disturbance acceleration calculations, providing solutions comparable to real ones for machines with limited computational capacity.

2. Mathematic model

Consider a celestial body modeled as a sphere, with a reference system centered at the sphere's center and an arbitrary right-handed orthonormal triad (x, y, z) of unit vectors ($\hat{i}$, $\hat{j}$, $\hat{k}$).
The gravitational potential for such a modeled celestial body is represented in spherical harmonics according to the following formula[2]:

$$U(r,\phi,\theta) = \frac{\mu}{r}(1+\sum_{l=1}^{\infty}(\frac{r_{cb}}{r})^l[\sum_{m=0}^{l}(C_{l,m}\cos m\phi + S_{l,m}\sin m\phi)P_{l,m}(\sin\theta)] \tag{1}$$

where:
μ gravitational parameter of the celestial body
r_{cb} mean equatorial radius of celestial body
l,m order and degree of the harmonic expansion
r distance of orbiting body wrt center of celestial body
$C_{l,m}$, $S_{l,m}$ zonal, sectorial and tesseral harmonic coefficients
$\vec{r}$ = r$\hat{R}$ position vector
θ angle between $\vec{r}$ and its x-y projection
ϕ angle between positive x axis and $\vec{r}$ x-y projection
$P_{l,m}$ associated Legendre functions, defined as:

$$P_{l,m}(x) = \frac{(-1)^m}{2^l l!}(1-x)^{\frac{m}{2}}\frac{d^{l+m}}{dx^{l+m}}(x^2-1)^l \tag{2}$$

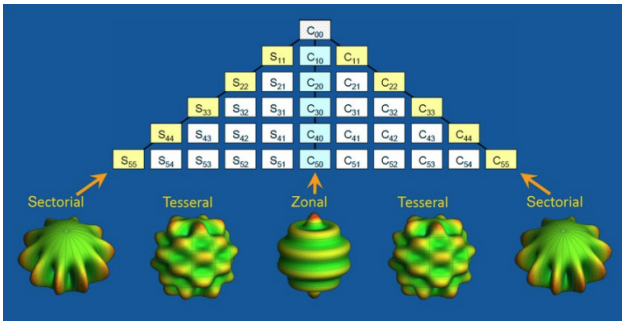

Figure 1: Visual representation of the zonal, sectorial and tesseral harmonics

Through the gradient of the potential, the gravitational acceleration acting on the orbiting body is obtained:

$$\vec{a} = \nabla U = \frac{\delta U}{\delta r}dr + \frac{\delta U}{\delta \sin\theta}d\sin\theta + \frac{\delta U}{\delta\phi}d\phi \tag{3}$$

This formulation, however, exhibits singularities.
The gradient

$$d\phi = \frac{1}{r(1-sin^2(\theta))}\hat{k}\times\hat{R}$$

becomes indeterminate as $\theta \to \pm 90$ since:

$$1-sin^2(\theta)\to 0 \quad \hat{k}\times\hat{R}\to 0$$

Due to the arbitrariness of the triad, this singularity cannot be eliminated by rotations of the reference system. Additionally, the first derivatives

$$\frac{dP_{l,1}(sin(\theta))}{dsin(\theta)}$$

ddiverge to infinity due to the derivative of the term $(1-\sin^2\theta)^{\frac{m}{2}}$ evaluated at m=1, $\theta \pm 90$

2.1. Pines formulation

To address the presence of singularities, the following considerations are made:

$$s = x/r \quad t = y/r \quad u = z/r = \sin\theta$$

direct cosine components of the position vector with respect to the x, y, and z axes. We introduce:

$$A_{l,m}(u) = \frac{1}{2^l l}\frac{d^{l+m}}{d(u)^{l+m}}(u^2-1)$$

and considering $(1-\sin^2\theta)^{\frac{m}{2}} = \cos^m\theta$ the summatory in m is rewritten as

$$\sum_{m=0}^{l}(C_{l,m}\cos^m\theta\cos m\phi + S_{l,m}\cos^m\theta\sin m\phi)A_{l,m}(u)$$

Considering the complex number:

$$\zeta = \cos\theta e^{i\phi} = \cos\theta(\cos\phi + i\sin\phi)$$

Through considerations of spherical trigonometry, one can relate ζ with direct cosines *s* and *t*:

$$\zeta = s + it \tag{4}$$

From the de Moivre's formula, it follows that

$$\zeta^m = \cos^m\theta(\cos m\phi + i\sin m\phi)$$

we then introduce

$$r_m = \mathsf{Re}(\zeta^m) \quad i_m = \mathsf{Im}(\zeta^m)$$

arriving at the expression of the gravitational potential according to Pines.[3]:

$$U(r,s,t,u) =$$
$$\frac{\mu}{r}(1+\sum_{l=1}^{\infty}(\frac{r_{cb}}{r})^l[\sum_{m=0}^{l}(C_{l,m}r_m(s,t)+S_{l,m}i_m(s,t))A_{l,m}(u)] \tag{5}$$

This formulation has the only singularity at r=0, a value that is non-physical considering that the expansion in spherical harmonics is valid only outside the central body.
Expanding the gradient of the potential, the acceleration acting on the orbiting body is finally obtained:

$$\vec{a} = (\frac{\delta U}{\delta r} - \frac{s}{r}\frac{\delta U}{\delta s} - \frac{t}{r}\frac{\delta U}{\delta t} - \frac{u}{r}\frac{\delta U}{\delta u})\hat{r} + (\frac{1}{r}\frac{\delta U}{\delta s}, \frac{1}{r}\frac{\delta U}{\delta t}, \frac{1}{r}\frac{\delta U}{\delta u})^T \tag{6}$$

3. Pines algorithm analysis

Considering the formulation presented in MathSpec[4] of the General Mission Analysis Tool (GMAT) application.
The computation of the disturbance acceleration is defined as follows:

$$(\frac{\delta U}{\delta r} - \frac{s}{r}\frac{\delta U}{\delta s} - \frac{t}{r}\frac{\delta U}{\delta t} - \frac{u}{r}\frac{\delta U}{\delta u}) =$$
$$-\sum_{l}^{L}\frac{\rho_{l+1}}{r_{cb}}\sum_{m=0}^{l}\bar{A}_{l+1,m+1}c_{l+1,m+1}D_{l,m} \tag{7}$$

$$\frac{1}{r}\frac{\delta U}{\delta s} = \sum_{l}^{L}\frac{\rho_{l+1}}{r_{cb}}\sum_{m=0}^{l}\bar{A}_{l,m}E_{l,m}m \tag{8}$$

$$\frac{1}{r}\frac{\delta U}{\delta t} = \sum_{l}^{L}\frac{\rho_{l+1}}{r_{cb}}\sum_{m=0}^{l}\bar{A}_{l,m}F_{l,m}m \tag{9}$$

$$\frac{1}{r}\frac{\delta U}{\delta u} = \sum_{l}^{L}\frac{\rho_{l+1}}{r_{cb}}\sum_{m=0}^{l}\bar{A}_{l,m+1}c_{l,m+1}D_{l,m} \tag{10}$$

where:
L order of harmonic expansion
A it is calculated through a recursive relationship:

$$A_{l,m} = u[\frac{(2l+1)(2l-1)}{(l-m)(l+m)}]^{\frac{1}{2}}A_{l-1,m}$$
$$-[\frac{(2l+1)(l-m-1)(l+m+1)}{(2l-3)(l+m)(l-m)}]^{\frac{1}{2}}A_{l-2,m} \tag{11}$$

with initial values given by the diagonal, independent of *u*:

$$A_{0,0} = 1 \quad A_{l,l} = \sqrt{\frac{2l+1}{2l}}A_{l-1,l-1}$$

For numerical stability reasons, the associated Legendre derivative functions must be normalized. The normalization coefficients are defined as:

$$N_{l,m} = \sqrt{\frac{(l-m)!(2l+1)}{(l+m)!}} \tag{12}$$

Then:

$$\bar{A}_{l,m} = N_{l,m}A_{l,m} \quad \bar{C}_{l,m} = \frac{C_{l,m}}{N_{l,m}} \quad \bar{S}_{l,m} = \frac{S_{l,m}}{N_{l,m}}$$

Real and imaginary coefficients are computed through the following recursive relationships:

$$r_m = sr_{m-1} - ti_{m-1} \quad i_m = si_{m-1} + tr_{m-1}$$

From (4) the initial values are:

$$r_0 = 1 \quad i_0 = 0 \tag{13}$$

D, E, F auxiliary matrixes, with elements computed as:

$$D_{l,m} = C_{l,m}r_m + S_{l,m}i_m \tag{14}$$

$$E_{l,m} = C_{l,m}r_{m-1} + S_{l,m}i_{m-1} \tag{15}$$

$$F_{l,m} = S_{l,m}r_{m-1} - C_{l,m}i_{m-1} \tag{16}$$

Pines auxiliary variables:

$$\rho = r_{cb}/r \quad \rho_0 = \mu/r \quad \rho_l = \rho\rho_{l-1}$$

Corrective normalization coefficients for $A_{l,m+1}$ and $A_{l+1,m+1}$:

$$c_{l,m+1} = \sqrt{(l-m)(l+m+1)}$$

$$c_{l+1,m+1} = \sqrt{\frac{(l+m+2)(l+m+1)}{(2l+3)(2l+2)}}$$

4. Approaches to the Pines algorithm

During this thesis work, two types of approaches have been used for the computation of the disturbance acceleration, one based on an analytical solution and one approximate. With the first approach, the parallelization of the Pines algorithm is performed through the parallel calculation of the coefficients $D_{l,m}$ $E_{l,m}$ $F_{l,m}$ and their respective summations.
In the second approach, disks are defined corresponding to lunar mascons, approximating the gravitational potential to only include the contribution of zonal harmonics up to the 4th order outside of these disks. The second approach is then modified to improve precision in the areas surrounding the mascons.
For the Moon, the following are defined:
r_{moon} = 1737.4 km mean lunar equatorial radius
μ_{moon} = 4904.8695 $\frac{km^3}{s^2}$ lunar gravitational parameter

An orbit is taken as a reference, described by the following initial orbital parameters evaluated with respect to the lunar Body Fixed reference frame:
a = 1850 km **e** = 0 **i** = 45°
Ω = 163.8° ω = 0° ν = 201°
The average execution time of the generic algorithm is considered as

$$t = \frac{\sum_{n=1}^{N} t_n}{N}$$

with t_n the time taken to calculate the acceleration at the n-th point, where N is the number of evaluated points.
The exact solution is understood as the acceleration computed through the Pines algorithm with a spherical harmonics expansion to the highest order and degree for comparison at each orbital evaluation point.
The harmonic coefficients used are derived from the data obtained from the mission GRAIL[5], expanded until the 900° order and degree.

4.1. Parallelization of the Pines algorithm

In this approach, the goal is to parallelize the Pines algorithm by leveraging CUDA, an API developed by Nvidia for General Purpose GPU (GPGPU) Programming.
In this approach, the first step of the algorithm involves calculating the recursive relationships, which are not parallelizable, on the CPU. The matrix $\bar{A}$ is computed through the relationships (11) (12), and the vectors $r_m, ; i_m$ are computed through (13). These, along with $C_{l,m}$ and $S_{l,m}$, are then transferred to the GPU's VRAM (Video RAM).

The CUDA kernel is then invoked, where each thread determines its own values of l and m based on its threadIdx defined through the API. The calculations for (14), (15), (16) are performed, and the result is multiplied by the corresponding $\bar{A}_{l,m}$. The outcomes are summed within four shared buffers specifically allocated.

Once the kernel execution is complete, the buffers containing the summations in m are transferred to RAM, and on the CPU, the final summation in l is performed, leading to the accelerations (equations (7) - 10).
In Figure (2), the execution time ($log_{10}(\mu s)$) of the Pines algorithm on both the CPU and GPU for various orders and degrees is shown. As evident, the parallel approach is orders of magnitude slower than the same algorithm executed on the CPU. This is mainly attributed to the latencies introduced by data transfers between RAM and VRAM and vice versa.
To benefit from a parallel approach, a substantial amount of parallelizable computations is required to make the latencies introduced by memory transfers favorable compared to CPU computation times.
Developments in this direction are presented in *J.R. Martin, GPGPU Implementation of Pines' spherical harmonic gravity model*(2021)[6], where the possibility of parallelizing the Pines algorithm for multiple orbiting bodies is analyzed.

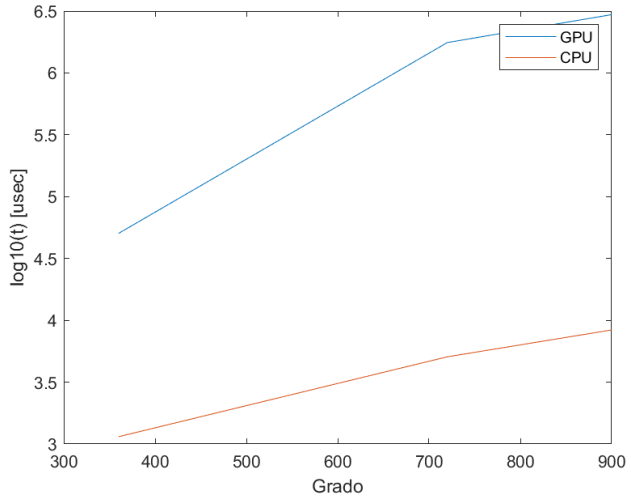

Figure 2: Tempi di esecuzione dell'algoritmo di Pines di CPU e GPU

Mascon	θ_d	ϕ_d	Diametro (km)
Mare Imbrium	32.8 N	15.6 W	1146
Mare Serenitatis	28 N	17.5 E	674
Mare Crisium	17 N	59.1 E	556
Mare Orientale	19.4 S	92.8 W	294

Table 1: List of considered seas, their relative coordinates of the central point, and diameters:

This involves increasing the number of computations necessary for solving the problem, making a parallel approach advantageous.

4.2. Disk approach

Another possible approach is to approximate the mascons as disks on the lunar surface.

In Table (1), the considered mascons are listed, specifying the coordinates of the center and their respective diameters. In Figure (3), these mascons are identified on the lunar surface.

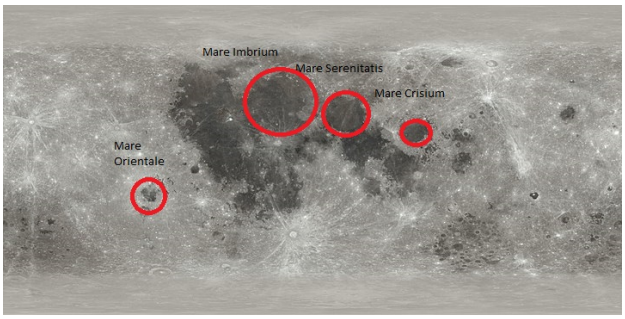

Figure 3: Position of seas in Table (1) on the lunar surface

Then, the distance from the center of the mascon to the point under the satellite is calculated as:

$$\text{dist}_{SSP,d} = 2r_{moon}sin^{-1}(\frac{sin(\theta_{SSP}-\theta_d)^2}{2}+$$

$$+cos(\theta_d)cos(\theta_{SSP})(\frac{sin(\phi_{SSP}-\phi_d)^2}{2})) \quad (17)$$

with:
θ_{SSP} latitude of sub satellite point
ϕ_{SSP} longitude of sub satellite point
The calculated distance is then compared with the radius of the disk r_d.
If

$$r_d \geq \text{dist}_{SSP,m}$$

the point under the satellite falls inside the disk. Therefore, the potential is calculated as in equation (5) with degree l_d, obtaining the acceleration through the Pines algorithm.

If

$$r_d < \text{dist}_{SSP,m}$$

The point under the satellite falls outside the disk, and only the contribution of zonal harmonics up to the 4th degree is considered for acceleration.

In Figure (4), the absolute error between the magnitudes of the accelerations approximated with the disk algorithm and the exact accelerations calculated for each orbit evaluation point is shown.
The most significant source of error comes from unmodeled or poorly modeled areas of mass concentration, such

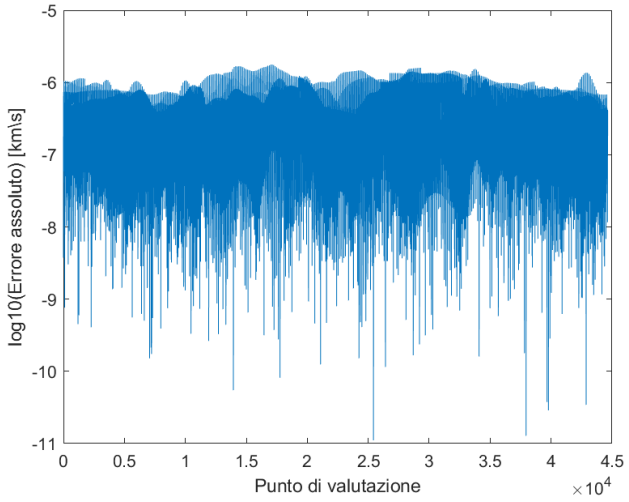

Figure 4: Absolute error between the exact solution and the approximate disk algorithm solution for l_d = 360

as disks where only the contribution of zonal harmonics up to the 4th degree is considered.

The maximum absolute error is on the order of 10^{-6} km/s^2. Accelerations of this magnitude are not negligible.
For illustrative purposes, Figure 5 shows the variation of the major axis of the reference orbit calculated with the disk algorithm and that derived from the exact solution for l_d = 360. As can be seen, the two results diverge rapidly from the beginning, demonstrating the inadequacy of the solution obtained using the disk algorithm.

[Note: For this case an rk45 integrator is used for orbit propagation, as the standard Adams-Bashforth-Moulton algorithm used for orbital integration kept failing at error control]

However, the disk algorithm has an average execution time t_d much lower than the computation of the solution integrated with the Pines algorithm for a degree l_d (Table (2)). The algorithm allows a reduction in computation times by a factor of 14. It is therefore necessary to attempt to improve the approximation without significantly affecting the execution times.

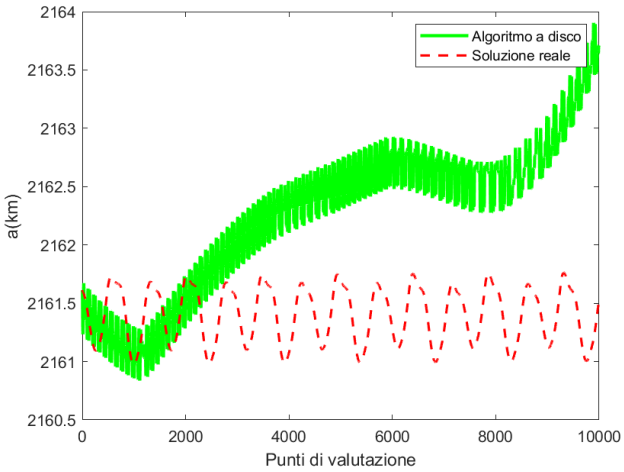

Figure 5: Variation of the major axis of the reference orbit for l_d = 360:

4.2.1. Modified disk approach

To improve the approximation of the disk algorithm, a gravitational influence zone outside the considered mascons is modeled as a second disk with a radius of $r_{d,roi} = 1.5r_d$, centered at the same point as the mascon.
If

$$r_d < \text{dist}_{SSP,d} \leq r_{d,roi}$$

the point under the satellite is outside the disk but within its gravitational influence zone. In this zone, the potential is partially developed with an order l_{roi} of spherical harmonics, half of that developed inside the mascon (l_m). Additionally, to reduce the error in the unmodeled areas outside the mascons and influence zones, an order l_{ext} is considered, which is half of l_{roi}. Therefore:

$$l_{roi} = l_m/2, \quad l_{ext} = l_{roi}/2$$

where l_m, l_{roi}, l_{ext} respectively, orders of spherical harmonics inside the disks, inside the influence zones, and outside. The order of magnitude of the absolute errors for

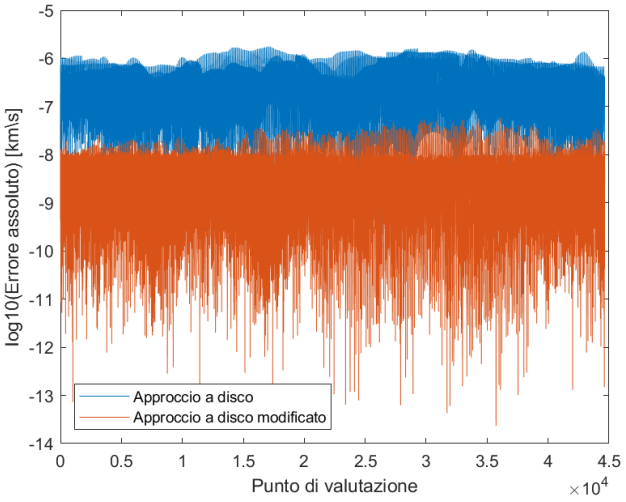

Figure 6: Comparison of the absolute error (log10) between the disk algorithm and the modified disk algorithm on the orbit evaluation points:

the disk algorithm and the modified disk algorithm is presented in Figure 6.

As can be observed, at least two orders of magnitude in precision are gained with a much lower computational time compared to the computation of the exact solution.

As an illustrative example, Figure 7 shows the variation of the major axis of the reference orbit calculated with the modified disk algorithm and that derived from the exact solution using the Pines algorithm with degree l_m = 360. It can be observed that the solution derived from the modified disk algorithm is comparable to that derived from the exact solution.

The average execution time of the modified disk algorithm t_{dm} remains lower than t_p by almost an order of magnitude for each degree (Table 2), resulting in a reduction in computation times by a factor of 8-10.

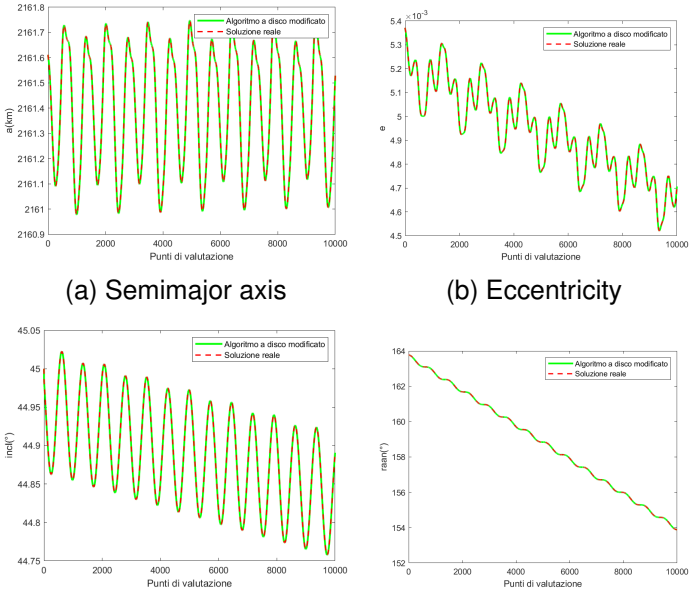

(a) Semimajor axis (b) Eccentricity

(c) Inclination (d) RAAN

Figure 7: Orbital parameters variation for l_m = 360

Algoritmo	*360*	720	900
serial	1146 μs	5012 μs	8360 μs
parallel	194 ms	1741 ms	2996 ms
Disk	78 μs	315 μs	503 μs
Modified disk	153 μs	605 μs	1005 μs

Table 2: Average execution times for the disturbance acceleration calculation for various orders and degrees.

5. Conclusions

Despite the parallel algorithm providing an accurate solution, its significantly higher execution times compared to the serial counterpart for each order and degree make it disadvantageous for real-time calculations.
On the other hand, the excessively approximate solutions of the disk algorithm make it inadequate for high-precision calculations despite its high computational speed, 14 times faster than the computation of the exact solution (Table (2)). Comparable results to the exact solution are obtained with the modified disk algorithm while maintaining high

execution speed compared to the computation of the exact solution. Further studies may lead to improved algorithm execution times by searching for optimal values for l_{roi} e l_{ext}.

References

[1] https://pgda.gsfc.nasa.gov/products/50

[2] Genova, A., Space Exploration Systems - Orbit Perturbations, presentazione, 2021

[3] Pines, S, Representation of the Gravitational Potential and its derivatives, *AIAA*, vol. 11, no.11, 1973.

[4] https://gmat.sourceforge.net/docs/R2020a /GMAT-MathSpec.pdf pag 86-89

[5] https://pds-geosciences.wustl.edu/grail/grail-l-lgrs-5-rdr-v1/grail_1001/shadr/gggrx_0900c_sha.tab

[6] J. R. Martin and H. Schaub, GPGPU Implementation of Pines' spherical harmonic gravity model, 2021.